



Long-term changes in sea-level components in Latin America and the Caribbean

I.J. Losada ^{*}, B.G. Reguero, F.J. Méndez, S. Castanedo, A.J. Abascal, R. Minguez

Environmental Hydraulics Institute "IH Cantabria", Universidad de Cantabria, Spain

ARTICLE INFO

Article history:

Received 19 September 2012

Accepted 19 February 2013

Available online 26 February 2013

Keywords:

inter-annual variability

Latin America and the Caribbean

sea-level components

sea-level rise

storm surge

non-stationary extremes

ABSTRACT

When considering the threat of rising sea-levels, one must take into account not only the changes in the Mean Sea-Level, but also storm surges and changes in extreme events which may also have a bearing on coastal problems. In this study, we combine different components of the total sea-level (astronomical tide, monthly mean sea-level and storm surges) to explain changes detected in the region of Latin America and the Caribbean. Methods based on non-stationary extreme value analysis were applied to storm surge and total sea elevations monthly maxima for the last six decades, while long-term trends in Mean Sea-level were computed from both local regression and a trend-EOF technique. In addition, the relative importance of each factor contributing to the total sea-level is explored by means of defining each statistical distribution. The analysis demonstrates that concerns should be focused on the different components of sea-level in the various areas of the region. For example, changes in the storm surge levels are a key stressor in the Río de la Plata area, while the increase in the extreme total sea-levels in the tropical region and the influence of inter-annual variability on its western coast are the prominent factors. Results show that a clear correspondence between Mean Sea-Level and the Niño3 climate index can be found through a simple regression model, explaining more than 65% of the variance for a representative location on the Peruvian coast.

© 2013 Elsevier B.V. All rights reserved.

1. Introduction

Coastal zones are among the most vulnerable areas to climate change and they are likely to be affected by various impacts in the foreseeable future. Among these, rising sea-levels, sometimes combined with land subsidence, have been highlighted as one of the key threats, which may lead to flooding, coastline erosion, impacts on ecosystems and salination of aquifers (Ericson et al., 2006; Syvitski et al., 2009; Nicholls and Cazenave, 2010). As a result, such problems have mandated action being taken for adaptation and integrated coastal management (e.g., Nicholls, 2011). However, the first step is to thoroughly understand the past changes in specific areas where the impacts are to be inferred, and with an adequate spatial scale. For this, a comprehensive understanding of the major factors contributing to total sea-level is required to lead efforts towards further analysis, prevention, and solutions to flooding and erosion. To this end, this work aims to offer a thorough examination of the different sea-level components in Latin America and the Caribbean region (LAC) and to define the long-term trends in the mean and extreme sea-levels.

In this work, time series of Total Sea-Level (TSL) results from the combination of four main components which vary both temporally and spatially:

- (1) Monthly mean sea-level (MSL): average height of the sea surface water level (Church et al., 2004), including the seasonal cycle (monthly mean) and the anomalies in time scales from the monthly variations (i.e. anomalies over the seasonal cycle) to the longer-term changes.
- (2) Astronomical tide (AT): sea level variation produced by the gravitational interactions of the earth, moon, and sun. In this work, the astronomical tide is calculated as the superposition of harmonic constituents provided by the TPXO database (i.e. eight primary (M2, S2, N2, K2, K1, O1, P1, Q1), two long period (Mf, Mm) and 3 non-linear (M4, MS4, MN4) harmonic constituents; long period constituents SA and SSA are not included).
- (3) Storm Surge (SS): water height above predicted astronomical tide level due to the inverse barometer effect and the wind stress over the sea surface.

Aggregation of the different components forms hourly TSL time series whose analysis may determine the probability of flooding on different time scales. One of the main objectives of this work is explaining the changes observed in the various sea-level components and analyzing the changes in the TSL extremes in the LAC region.

There are however, some additional components of sea level not covered by the former combination of components. For instance,

* Corresponding author at: Environmental Hydraulics Institute, IH Cantabria, Universidad de Cantabria, C/Isabel Torres nº 15, Parque Científico y Tecnológico de Cantabria, 39011, Santander, Spain. Tel.: +34 942 201414.

E-mail address: losadai@unican.es (I.J. Losada).

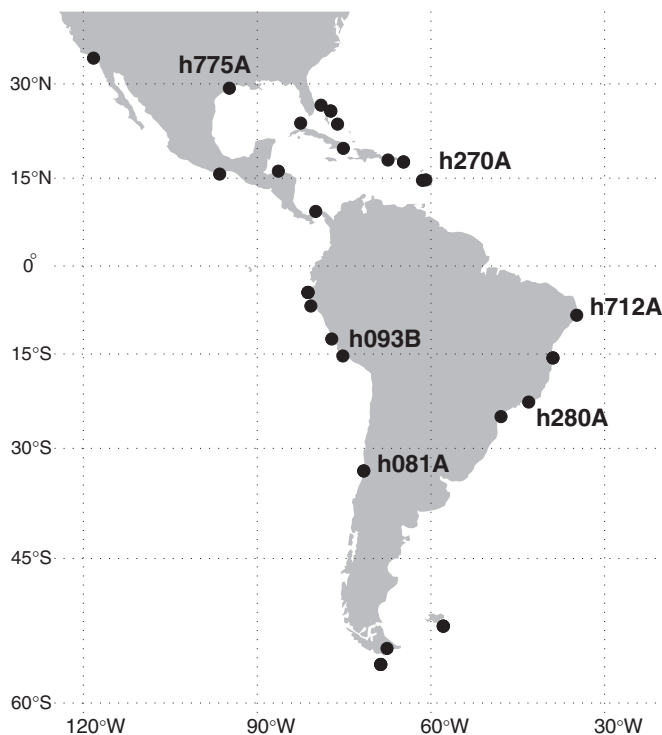


Fig. 1. The region of study, showing the tidal gauges selected for validation purposes.

breaking waves cause sea-level changes in the surf-zone (swell set-up), which depend on local coastal characteristics. This factor is not analyzed here however, since our main focus is on sea-level variations in deep waters and therefore local surf zones are not taken into account.

Sea-Level Rise (SLR) is the name given to changes in the MSL detected over many years. Rising sea-levels have been extensively studied in recent years (e.g., IPCC, 2007; Cazenave et al., 2008; Church and White, 2011; Rignott et al., 2011; or de Santis et al., 2012). Local factors such as land subsidence cause additional displacement to be added to the effect of SLR, the combination of which is known as Relative Sea-Level Rise (rSLR). Land subsidence was not considered in the analysis but it doubtlessly is a factor to consider at a local scale.

There are also variations of the MSL time series that are not represented by the long-term trend. Hereinafter, these sorts of anomalies are referred to as interannual variability. Under this term we analyze variations induced by ENSO events (e.g. Clarke and Van Gorder, 1994; Nerem et al., 1999; Li and Clarke, 2007) or other decadal-scale wind stress curl variability (e.g., Sturges and Hong, 1995; Sturges et al., 1998; Hong et al., 1999). Defining the influence of climatic patterns on different components of the sea-level at a continental scale has not been addressed so far and should be attended to since it may be relevant for coastal areas.

In spite of the great attention to the study of the SLR, the changes in sea-level extremes are the upshot of combinations between SLR, the

incidence of storms, local trends and the marine climate, as suggested in Walsh et al. (2012). The combination of rising sea-levels and storm surges has already been dealt with at a global scale in several studies (Dasgupta et al., 2009), and specifically for particular areas of the LAC region (Fiore et al., 2009). Similarly, the effect of SLR on extreme sea-levels has also been addressed at a global scale (Menéndez and Woodworth, 2010). However, identifying specific coastal locations where one or more components (changes in mean sea level, astronomical tide, storm surge, inter-annual change) may be dominant is crucial. For instance, sea-level extremes occur not only under high SS values independently of the AT component, but high rises due to AT and moderate SS values may eventually pose a flooding risk on particular coasts. This is why this study ends with a discussion of the relative importance of each of the contributing factors for the particular region of LAC using homogenous data for the whole of the region.

The structure of the work is as follows. The section following this introduction describes the regional setting of the work. The data sources and the statistical methods used for the extremes analysis and the study of the long-term trends are explained in Section 3. Section 4 deals specifically with the study of sea-level components, their changes, and their relative importance in different parts of the continent. A brief discussion of the climatic patterns with the highest influence on each component is provided in Section 5. Finally, Section 6 highlights the most important conclusions.

2. Regional setting

The area of study is the region of the Atlantic and Pacific Ocean basins that are adjacent to the coasts of LAC (see Fig. 1). With a total coastline length of about 72,182 km, this region is highly variable in terms of coastal dynamics and geomorphological features. In the Atlantic, Pacific and Caribbean shores, the conditions are highly variable and present particular features at each location. Generally, little knowledge is available on the different sea-level components and their past temporal changes over the region extending from the high latitudes in the Southern Ocean to the equatorial areas.

3. Data and methods

3.1. Data

Several sources of instrumental and numerical data were used to evaluate the sea-level components in the LAC region. Table 1 summarizes the variables considered and their original source, as well as their time span and spatial resolution.

MSL data were obtained from the Commonwealth Scientific and Industrial Research Organization (CSIRO) and can be downloaded at: http://www.cmar.csiro.au/sealevel/sl_data_cmar.html.

These data provide monthly MSL series on a $1^\circ \times 1^\circ$ (longitude \times latitude) grid of spatial resolution between 65°S and 65°N , from 1950 to 2001, reconstructed from tidal gauges (Church et al., 2004). The seasonal signal is removed from the dataset and it includes the inverse barometer correction and the GIA (Mitrovica) correction made to tidal gauge data. The relative movement between land and

Table 1

Sources of information of the variables considered, their time span and spatial resolution.

Data source	Variables	Time span	Time resolution	Spatial resolution
CSIRO	Mean Sea-level(MSL) Mean Sea-level anomaly	1950–2009	Monthly	Global, 1°
TPXO dataset (v7)	Astronomical Tide (AT)	Harmonic constants	Hourly	Global, 0.25°
Tidal gauges (UHSLC)	Mean Sea-level(MSL) Storm Surge (SS)	Variable	Hourly	Global, variable
Numerical reanalysis (GOS)	Storm Surge (SS)	1948–2008	Hourly	LAC, 0.25°

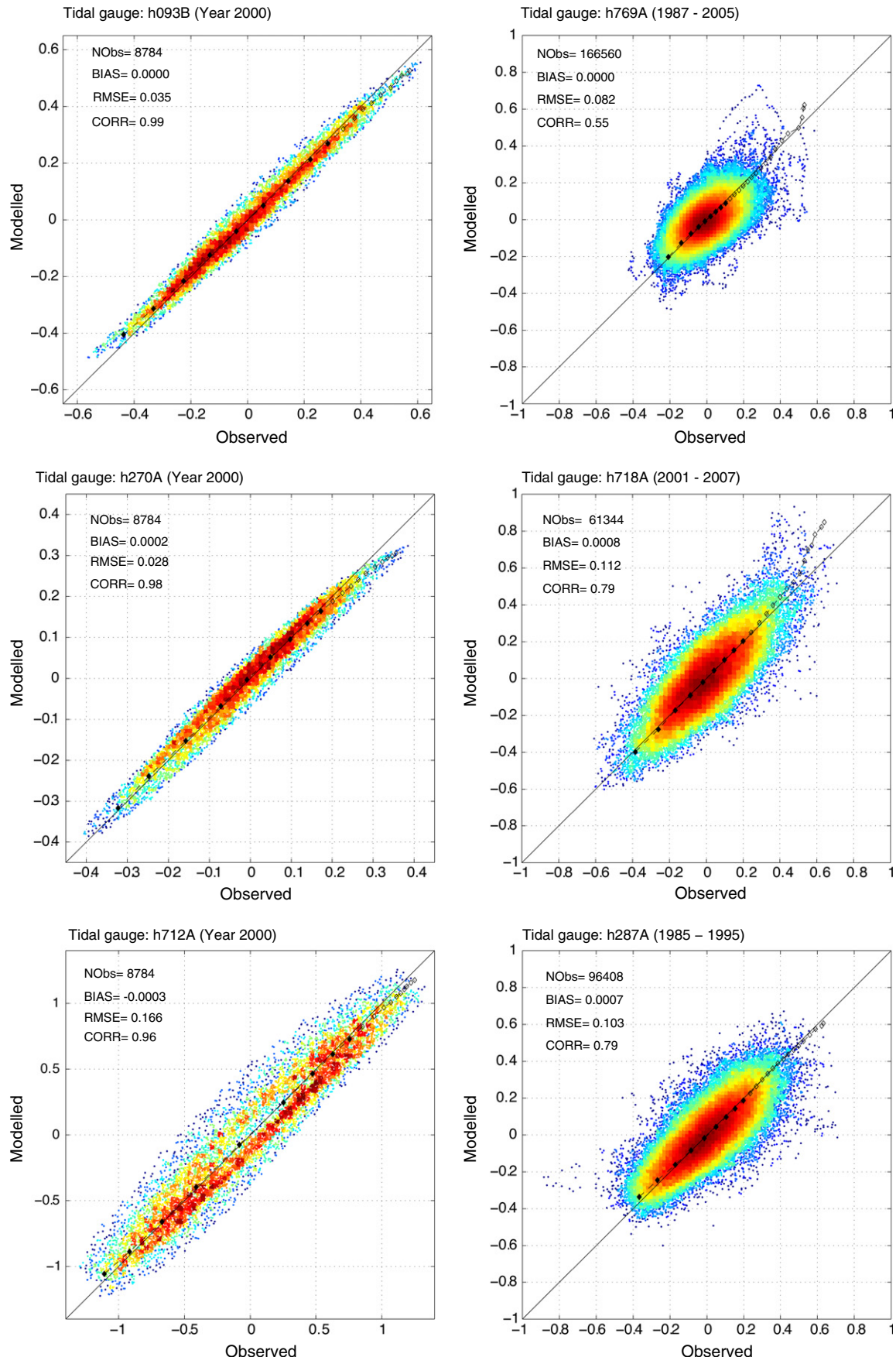


Fig. 2. Validation of the reconstruction of the Astronomical Tide (left) and the modeled Storm Surge (right) with various regional tidal gauges in the study area. Scatter data and quantile distribution are shown. Values expressed in meters.

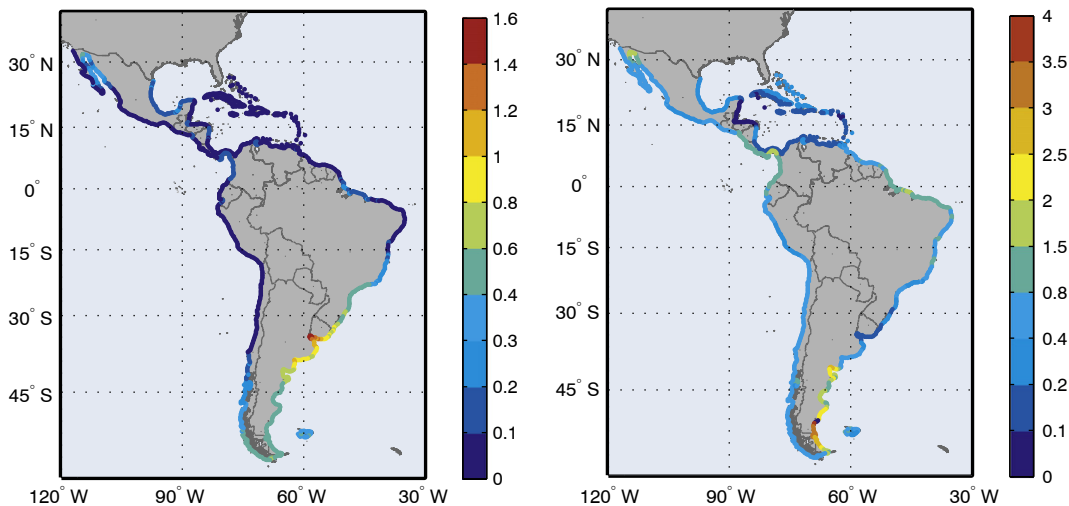


Fig. 3. Annual 99th percentile of Storm Surge (left panel) and 90th percentile of Astronomical Tide (right panel), computed for the period 1948–2008 and expressed in meters.

sea-level is not considered in the database. Data covering the period from 1993 to 2008 was also employed from TOPEX/Poseidon, Jason-1 and Jason-2/OSTM altimeters.

Tidal gauge data were obtained from Hawaii University's Sea-level Center (UHSLC) and used to compare the results of the AT and the SS time series. These data are available at <http://ilikai.soest.hawaii.edu/uhscl/rqds.html>. Locations are presented in Fig. 1, along with the identification codes of the tidal gauges shown in this paper for validation. The data series provides hourly time resolution, and registers longitude variations for each station.

AT data were generated on the LAC coasts using the harmonic constants derived from the TPXO global tides model (version 7) developed by Oregon State University (Egbert et al., 1994; Egbert and Erofeeva, 2002). The TPXO model assimilates data from the TOPEX/Poseidon missions and tidal gauges (Ardalan and Hashemi-Farahani, 2007). The database includes eight primary harmonic constants (M_2 , S_2 , N_2 , K_2 , K_1 , O_1 , P_1 , Q_1) and two long period ones (M_F and M_m), provided in a global grid of 1440×721 points, at 0.25° spatial resolution (<http://volkov.oce.orst.edu/tides/global.html>). These components were used to reconstruct the hourly AT series beginning in 1948. Results were validated using the area tidal gauges (see Fig. 2) with root mean square errors of less than 0.2 cm (at macro-tidal regimes, lower in micro-tidal sites), so that reconstructions of the AT can be considered adequate for offshore depths. The distribution of the 90th percentile of AT is shown in Fig. 3 (right panel) and the region's great spatial variation is clear, with microtidal regimes in tropical latitudes, and macrotidal ones in the south.

Storm surge was obtained numerically using the Regional Ocean Modeling System (ROMS) (Shchepetkin and MacWilliams, 2003) at $0.25^\circ \times 0.25^\circ$ resolution, from 125°W to 20°W longitude and 61°S to 40°N latitude. We used the inverse barometer condition and obtained atmospheric forcing (pressure and wind data) from NCEP/NCAR reanalysis (Kalnay et al., 1996), resulting in hourly time series of storm surge for the period from 1948 to 2008. The run was performed with only atmospheric forcing (similarly to e.g., McInnes et al., 2009), although an alternative approach would be to run the tides and atmospheric forcing together, and then subtracting the values from a tide-only run (as shown in Lowe and Gregory, 2005). Note however, that non-linear tide-surge interaction mainly occurs at wide shelves in shallow areas, which requires high spatial resolution, i.e. $O(1\text{--}5\text{ km})$. Owing to the spatial scale of the present work this non-linear effect cannot be properly modeled.

The results were validated with instrumental tidal gauge data. Fig. 2 shows the results of the validation for several tidal gauges in

the zone. A good fit for both the statistical distribution and surge time series (not shown) has been obtained. The panels show the scatter, quantile-quantile plot, and statistical diagnostic indices of observed versus modeled data. Colors indicate the sample density. The solid line corresponds to modeled data equal to observed data ($y = x$). Non-filled points show quantiles higher than the 90th percentile. We also show the data number in the dataset (NObs), the BIAS (mean (y) – mean (x)), RMSE (the root mean square error) and the Pearson's correlation coefficient (CORR). It should be noted that this dataset does not include hurricanes, which define the SS extremes tail, because of the insufficient resolution of the NCEP/NCAR wind and pressure reanalysis. An accurate definition of hurricanes requires a specific analysis which could not be included in this work without loss of generality for the results in the region covered.

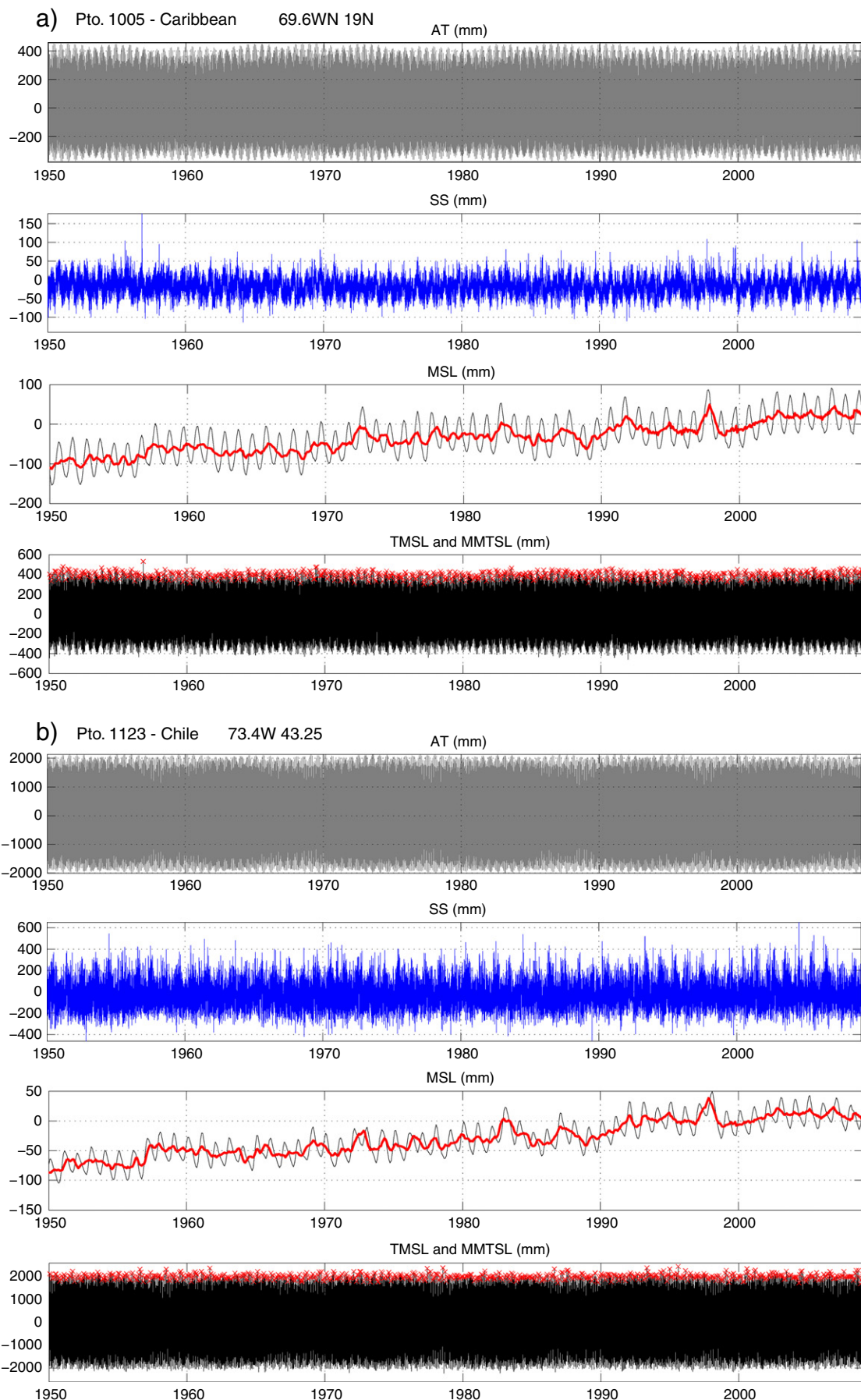
In Fig. 3 (left) the SS 99th percentile along the coast under study is presented. A large spatial variation in SS can be seen throughout the region. The highest values (over 1 m) are clearly found in the Río de la Plata area, a shallow platform where water accumulates during storm events. In general, the highest values are found in the southern part of the continent, particularly along the Atlantic coast. On the Pacific coast, north of the 35° S parallel, the storm surge of the 99th percentile is about 10 cm almost throughout the whole region, except in areas like the Gulf of California and the Colombian coast, where higher values are found. In this regard, it must be emphasized that local amplifications due to coastal zone local geometry and bathymetry demand greater spatial resolution, which is beyond the scope of this study.

By aggregating the components of AT and SS to the MSL series, it is possible to reconstruct the TSL series for two specific points in the region, as shown in Fig. 4. The first point is on the Chilean coast, where a semidiurnal tidal pattern is dominant, while the second one is found on the Caribbean coast, where tides are mixed and the tidal range is smaller. The weight of each component at each location differs distinctly. This aspect is analyzed in section 3.3, along with the comparison with the SLR trends.

3.2. Statistical methods

3.2.1. Long-term trends

The long-term variability of geophysical variables is generally described by calculating regional trends or using global averages. The evaluation of trends and their spatial-variability is a difficult problem, and trends have been detected using both linear and non-linear methods,



even with discontinuous datasets (e.g., Jevrejeva et al., 2006; Barbosa, 2008; Barbosa and Andersen, 2009; Church and White, 2011; Gazeaux et al., 2011). However, such methods generally only consider the temporal structure, neglecting the spatial influence on them when estimating trends. Moreover, trend detection is sensitive to the record length and the variance of the signal, among other factors (see Weatherhead et al., 1998; Weatherhead et al., 2002; Whiteman et al., 2011). For this reason, the influence of the ENSO in the signals should be taken into account, as they may affect the calculation of the trend (Lawrence et al., 2004; Becker et al. 2012).

Based on the foregoing considerations, we decided to use two different techniques, which in our opinion are simple to implement and allows for representation of the differences between local and regional evolution. Note that although the application of linear regression techniques at specific locations is a very simple procedure, it has several shortcomings:

- a) It may present discrepancies between records on close locations, i.e. it does not consider the spatial component.
- b) It is sensitive to the record length and the variance of the signal. This effect is important in this particular case because the variance of the signal in areas where the “el Niño” influence is relevant is comparatively higher than in the rest of the study area, and this may distort results.

Attempts are made to overcome these difficulties using techniques based on Empirical Orthogonal Functions (EOF; Fukuoka, 1951), by decomposing a continuous space-time field into an optimal set of basic functions of space, and expansion functions of time. However conventional EOF analysis is in general unable to find trends (Hannachi, 2007) since a substantial part of the signal variance is distributed into the different spatial-temporal modes. Hannachi (2007) found a modification of traditional EOF analysis to overcome this limitation (henceforth Trend-EOF).

The method is based on an eigen-analysis of the covariance matrix, similar to conventional EOFs, but taking the time positions of the sorted observations (named as inverted ranks) instead of the direct observations. The different sequences of inverse ranks provide a robust measure of monotonicity. Therefore, maximization of monotonicity can be obtained from maximization of the variance of a linear combination of the inverse ranks, ultimately leading to the identification of robust spatial-temporal trend patterns. This technique has already been used successfully for other geophysical variables (see Barbosa and Andersen, 2009).

In this work, the Trend-EOF technique was used to determine past changes in regional MSL, and to compare the results with those obtained by linear regression of the time series. Regarding the statistical significance of the regression models, it is based on the *t*-test. We check the null hypothesis $H_0: \beta_i = 0$ against the alternative hypothesis

H1. $\beta_i \neq 0$

The statistic is defined as $\frac{t=\hat{\beta}_i}{s_{\hat{\beta}_i}}$, where $s_{\hat{\beta}_i}$ corresponds to the estimated standard deviation of the parameter. The null hypothesis is rejected if $t \geq t_{\alpha/2,n-p}$ or $t \leq -t_{\alpha/2,n-p}$ where α is the significance level, and $t_{\alpha/2,n-p}$ is the quantile associated with the *t*-student distribution with $n-p$ degrees of freedom.

3.2.2. Extreme value analysis

The use of non-stationary extreme value models is widely accepted in the literature as a way to i) improve the characterization of the distribution tails, and ii) increase the understanding of which processes are important in the definition of extremes. Recent advances in the extreme value theory (see Coles, 2001 and Katz

et al., 2002 as general references) allow for modeling of the natural variability of extreme events of environmental and geophysical variables. These methods introduce time-dependent variations within a certain time scale (year, season or month), improving our knowledge of some important processes which are time dependent. Additionally, a key issue is the possibility of constructing regression models to show how the variables of interest may depend on other measured covariates. The statistical model proposed for this study is based on a generalized extreme value (GEV) distribution. The GEV model works with a sample of maximum values from blocks of equal temporal length. We defined the block span as a month, which provides a better description of extreme sea-level events within a year, allowing us to analyze the seasonal scale of interest. These maxima blocks are often assumed to be independent and identically distributed random variables, but natural climate variability induces changes in the monthly maxima. This fact contradicts the hypothesis of homogeneity in consecutive months, therefore a non-stationary approach was used.

In this particular case, the parameters were obtained through a maximum likelihood estimation method. The only difference with a stationary case is that we use a regression model for the location and scale GEV parameters that depend on time. This parameterization facilitates us working with monthly maxima instead of annual maxima, i.e. we use more information for the tail definition. This strategy, besides improving the characterization of maxima within the year, provides consistent results in terms of annual maxima, and has been proven to reduce uncertainty in quantile estimation (see Menéndez et al., 2009). This version of the GEV distribution has been recently used for different geophysical variables (e.g., Rust et al., 2009; Menéndez and Woodworth, 2010; Izaguirre et al., 2011). Thereby, we consider a time-dependent extreme model characterized by time-dependent location $\mu(t)$ and $\psi(t)$ scale parameters of the GEV distribution. The GEV cumulative distribution function of a certain random variable, Z_t , is given by:

$$F_t(z) = \begin{cases} \exp\left\{-\left[1 + \xi\left(\frac{z-\mu(t)}{\psi(t)}\right)\right]^{+}^{-1/\xi}\right\} & \xi \neq 0 \\ \exp\left\{-\exp\left[-\left(\frac{z-\mu(t)}{\psi(t)}\right)\right]\right\} & \xi = 0 \end{cases} \quad (1)$$

where $[a]_+ = \max[a, 0]$ and ξ is the shape parameter which informs us about the tail of the distribution.

Confidence intervals are obtained assuming approximate normality for the maximum likelihood estimators, and using the delta method (Rice, 1994). Statistical significance is based on the *t*-test as explained for the trend detection.

Mean sea-level seasonal oscillations have been widely studied (e.g., Tsimplis and Woodworth, 1994) and at a continental scale they are presumed to differ greatly among locations. In this approach, seasonal variability is explicitly modeled by allowing annual and semiannual cycles in location and scale parameters. Menéndez and Woodworth (2010) studied extreme sea-level events from a global dataset of tidal gauges using this approach with successful results. They found the simplest model with a minimum number of time-dependent parameters, through a stepwise procedure evaluating the final prediction error criterion (Menéndez et al., 2009; Minguez et al., 2010a). These techniques provide an automatic method of parameter selection which minimizes the Akaike Information Criterion (AIC). Incorporation of additional parameters at every iteration is based on sensitivity analysis and score test statistical information. The methods have proved to be efficient and robust, obtaining the best possible parameterization automatically.

Fig. 4. Reconstruction of Total Sea-Level time series (TSL) using the different components at two points in the study region: Caribbean coast (a) and Chilean coast (b). The series are shown for Astronomical Tide (AT), Storm Surge, Mean Sea-Level time series (MSL) and Total Sea-Level (TSL). The red line in MSL represents the annual mean values, while the red-cross line in TSL indicates the Monthly Maxima of Total Mean Sea-Level (MMTSL).

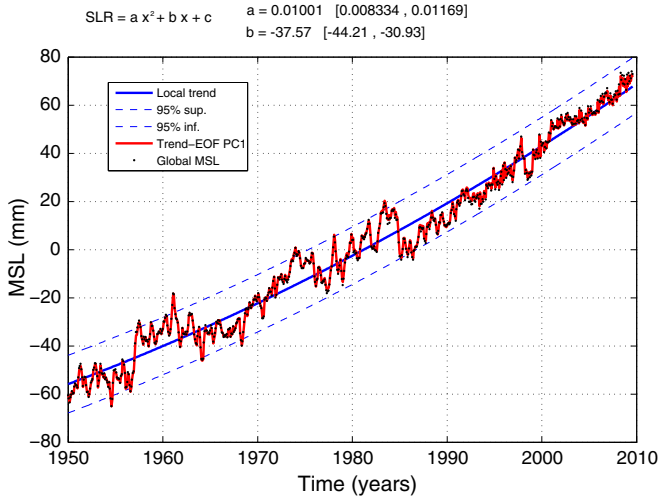


Fig. 5. Global mean sea-level trends. Trend derived from the First Trend-EOF component (red) along with the temporal instants of global mean sea-level (black points), trend adjusted with 95% confidence intervals (blue).

Accordingly, only significant sinusoidal functions (at 95% confidence levels) are included in the optimal model for each location (see Menéndez et al., 2009 and Minguez et al., 2010 for further details). The model used for the study of monthly TSL maxima follows:

$$\begin{aligned}\mu(t) &= \beta_0 + \sum_{i=1}^2 (\beta_{2i-1} \cos(i\omega t) + \beta_{2i} \sin(i\omega t)) + \beta_{LT} \cdot t \\ \psi(t) &= \alpha_0 + \sum_{i=1}^2 (\alpha_{2i-1} \cos(i\omega t) + \alpha_{2i} \sin(i\omega t)) + \alpha_{LT} \cdot t \\ \xi(t) &= \xi_0 + \sum_{i=1}^2 (\xi_{2i-1} \cos(i\omega t) + \xi_{2i} \sin(i\omega t))\end{aligned}\quad (2)$$

where β_0 and α_0 are mean values, β_i and α_i are the amplitudes of the harmonics, $\omega = 2\pi \text{ year}^{-1}$ and t is given in years. Thus stated, the model is able to simulate the increase or decrease, not only in the magnitude of the extreme events, but also in their variance. The

significance of each linear trend was computed using the likelihood ratio test.

To determine whether the SS showed different trend behavior within seasons, the model was modified by including the annual cycle in the term accounting for the long-term trend in the location parameter. The resultant model is expressed as:

$$\begin{aligned}\mu(t) &= \beta_0 + \sum_{i=1}^2 (\beta_{2i-1} \cos(i\omega t) + \beta_{2i} \sin(i\omega t)) + [\beta_{LT} + \beta_{LT1} \cos(\omega t) + \beta_{LT2} \sin(\omega t)] \cdot t \\ \psi(t) &= \alpha_0 + \sum_{i=1}^2 (\alpha_{2i-1} \cos(i\omega t) + \alpha_{2i} \sin(i\omega t)) + \alpha_{LT} \cdot t \\ \xi(t) &= \xi_0 + \sum_{i=1}^2 (\xi_{2i-1} \cos(i\omega t) + \xi_{2i} \sin(i\omega t))\end{aligned}\quad (3)$$

where β_{LT1} and β_{LT2} represent the amplitudes of the harmonics for the seasonal trends.

Extreme analysis of TSL (Eq. (2)) and SS (Eq. (3)) time series was performed applying the above methods, respectively. To report extreme value intensity, we chose a quantile of probability distribution, linked to a 50 year return level, which corresponds to a given no-exceedance probability of $1 - q$, with $q = 1/50$. It was obtained for each season by iteratively solving:

$$1 - q = \exp \left\{ -k_m \int_{t_a}^{t_b} \left[1 + \xi(t) \left(\frac{\bar{z}_q[t_1, t_2] - \mu(t)}{\psi(t)} \right) \right]^{-1/\xi(t)} dt \right\} \quad (4)$$

where $[t_a, t_b]$ is the interval equal to one season and $1/k_m$ is the length of the block maxima, that is, one season (3 months) so that $1/k_m = 1/4$ year. Details regarding the derivation of Eq. (3) can be found in Frías et al. (2012).

4. Study of sea-level components

4.1. Changes in mean sea-level

Two trend techniques have been used to study sea-level globally: the Trend-EOF and a trend based on linear regression of local time series. In both cases we used two regression models: a first ($z = at + b$) and a second ($z = at^2 + bt + c$) grade models. For the Trend-EOF regression, we made a regression analysis over the first

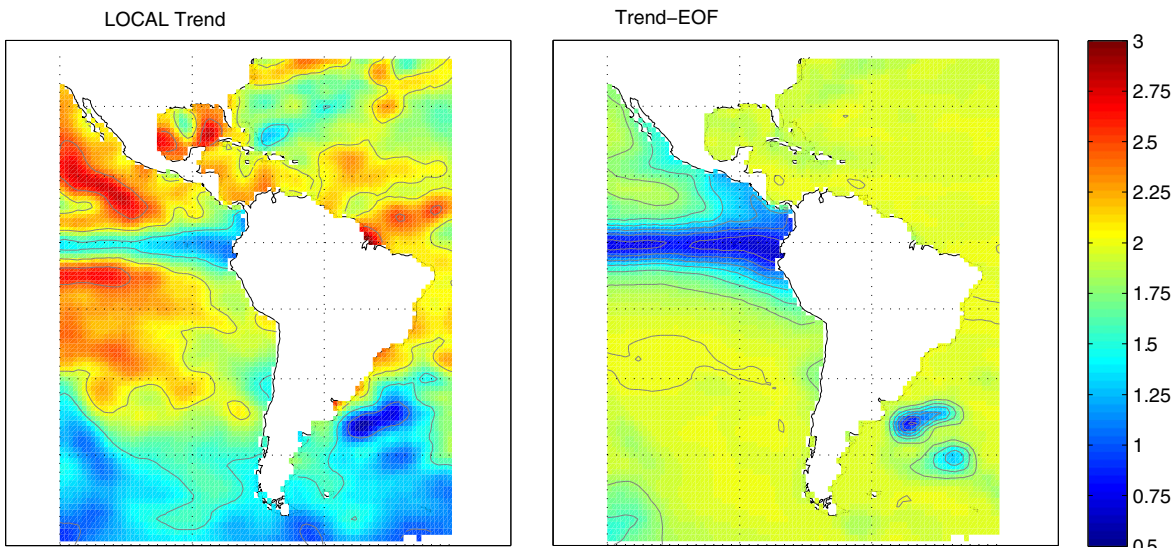


Fig. 6. Comparison of the Linear Trend of rising sea-level obtained by Local Regression (left) with the one obtained using the Trend-EOF technique (right) for the region of Latin America and the Caribbean (mm/year). Data analyzed for the period 1950–2008.

Principal component (i.e. representing the monicity of the signal), which is shown in Fig. 5 as a blue line, and projected this regression using the corresponding spatial mode.

Parameter estimation was performed using least-squares analysis, i.e. the parameters that minimize the sum of squares of the differences (errors) between the observed and predicted values. The solution of this problem is equal to the solution of the normal equations (see Chatterjee et al., 1990), which provide the expected values of the estimated parameters. Using the parameter estimates, and the variance-covariance matrix of parameter estimates, which is easily obtained using linear regression techniques, it is possible to check the null hypothesis as explained in the previous sections for trend detection and extreme analysis. Note that the same analysis also allows us to define where the linear and quadratic components were statistically significant.

Assessment of the minimum quadratic error proved the regression by both methods to be quadratic. This result suggests a mild acceleration of trends in the period 1950–2008. Fig. 5 shows the time series for average global sea level and the first component of the Trend-EOF (i.e.

that including the trend's global pattern), with a value of 2.7 mm/year in 2010 and a 0.01 mm/year² curvature. The statistical significance of our results was higher than 95%, and they are in accordance with previous trends calculated for mean global sea level (e.g., Church et al., 2004; Cazenave and Remy, 2011; Church and White, 2011; Becker et al., 2012; Meyssignac and Cazenave, 2012).

Fig. 6 shows the average trend calculated by both methods. Note that the trend-EOF technique allows the capturing of the main spatial trend, which yields results consistent with global mean sea level evolution, providing results less prone to short and/or high variance records, whereas local trends allows for observation of the local changes. However, where the variance of the signal is low, local trends may capture local variations that trend-EOF would overlook. If those changes are related to spatial variations of the trend signal or deficiencies, the analysis technique is more difficult to establish and this is a subject for further research.

The trend is clearly positive at all points, as shown in the various time series panels in Fig. 7. The highest values for these trends are found on the Atlantic coast: approximately 2 mm/year on the

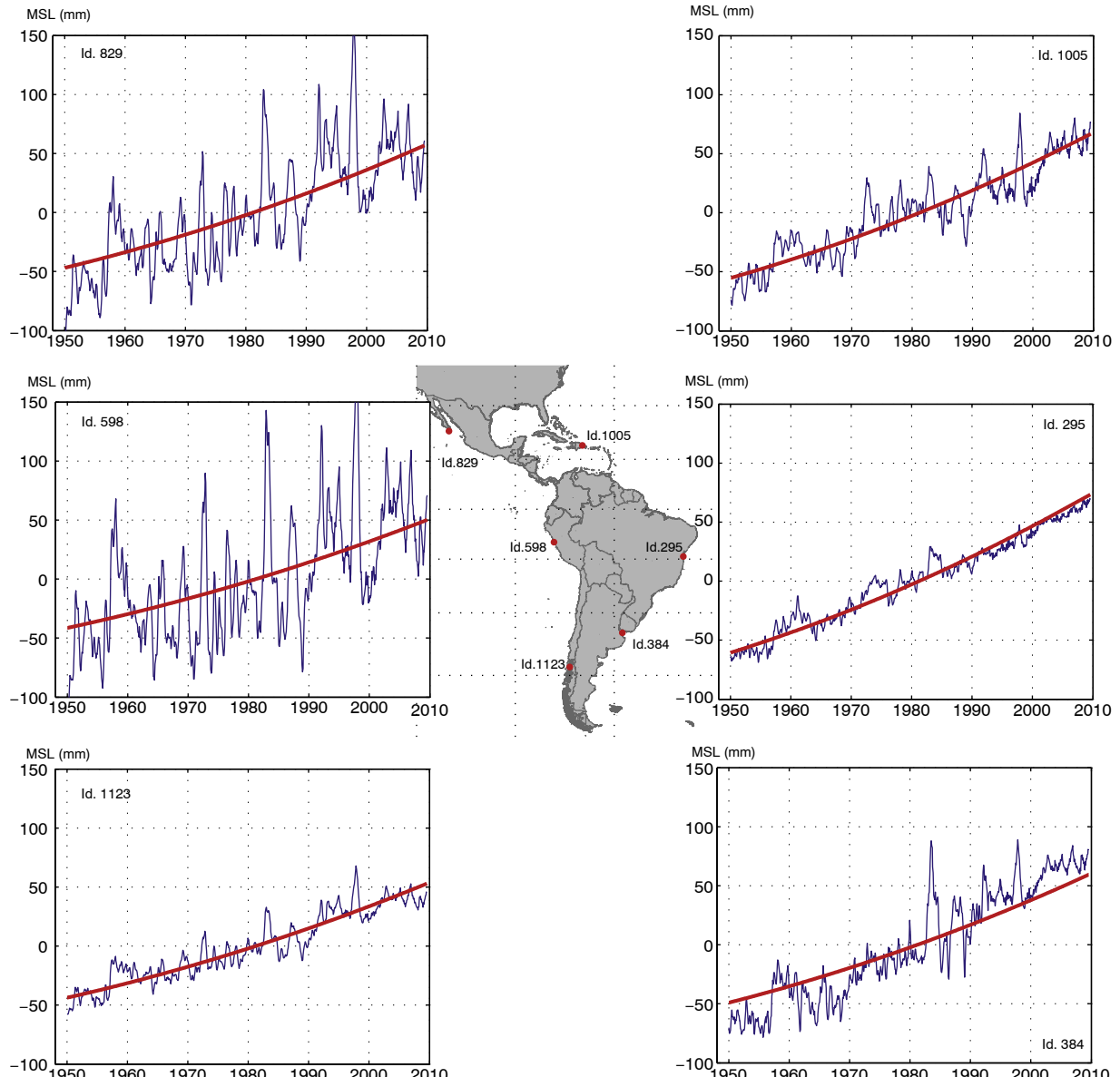


Fig. 7. Temporal series for rising sea-levels and the trends obtained (using Trend-EOF) for various representative points in study area.

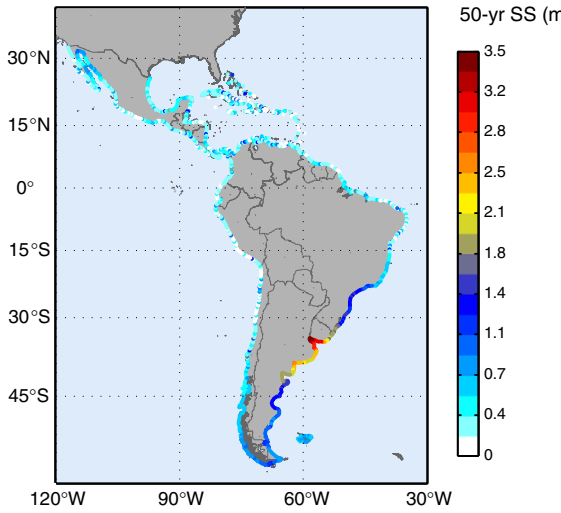


Fig. 8. 50-year return period Storm Surge height, obtained by hindcast from 1948 to 2008.

northern coast of South America and the Caribbean coast, with lower values in the Caribbean islands. In the equatorial Pacific area the increase is lower (1–1.5 mm/year). In addition, the influence of the ENSO phenomenon (periods of el Niño and la Niña) is seen in the

time series of anomalies, particularly along the Pacific coast, as will be analyzed in Section 4.

At this point it is worth comparing the effect of climatic variability on MSL over a multiple-year time scale, and the current long-term trend maintained in recent decades. Fig. 7 shows the different influence of el Niño and la Niña events on the Pacific coast of Central America, from Mexico to the coast of Peru. In 1998 (the Niño3 index historical high), the Niño3 index was at an historical high in the equatorial zone of the Pacific (not shown spatially but identified in Fig. 7 at point 598). If the sea-level time series are de-trended, it becomes possible to determine the effect of this event on MSL. A similar event would give values of around 20 cm at the point of maximum effect (considering only the effect on MSL and not the accumulated effects on other variables such as wave climate (see Reguero et al., 2012, 2013) or SS. This highlights the importance of studying all TSL components to discern the relative weight of changes to each component.

4.2. Changes in extreme storm surge levels

Extreme storm surge events decisively influence coastal flooding, making it essential to analyze them and their trends. An analysis of extremes of Storm Surges was performed, based on the GEV distribution and applied to the monthly maxima (see Eq. (3)) over the period from 1948 to 2008, making it possible to determine significant seasonal trends. Seasons were organized into three-month blocks: December, January, February (DJF); March, April, May (MAM); June, July, August (JJA); and September, October, November (SON).

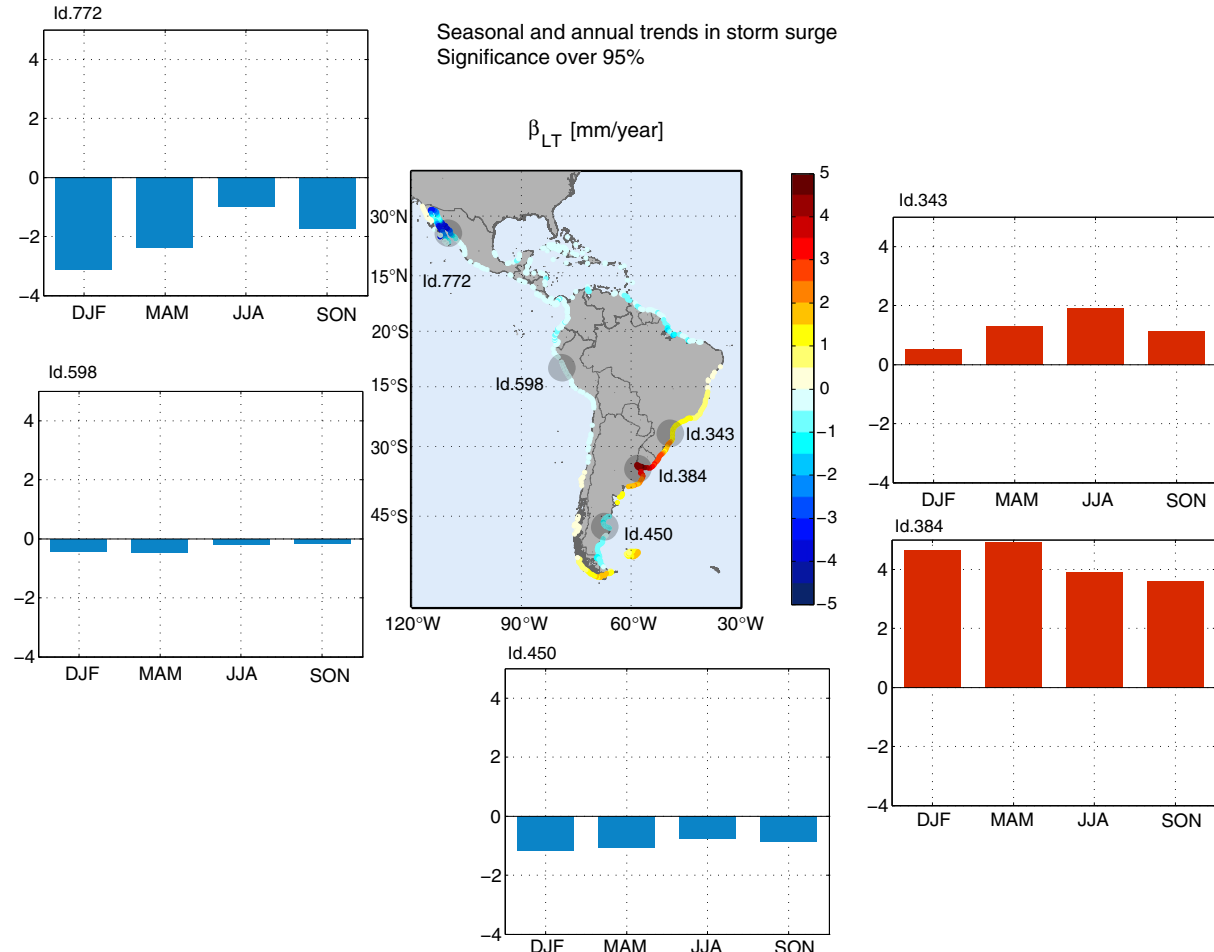


Fig. 9. Long-term trends in Storm Surge extremes excluding hurricanes and corresponding seasonal trends at some representative points (mm/year). The map in the center shows the annual trend while the adjacent panels represent the seasonal trends at the representative points marked in the map.

Hurricanes were not included in the dataset because of the lack of resolution in the pressure and wind fields in NCEP/NCAR reanalysis. Thus analysis in Central America and the Caribbean must be treated with caution because the magnitude of extreme values is not well represented, as the SS distribution tail is defined by these hurricane events.

Fig. 8 shows the 50 year return period SS. The highest values are found at the Río de la Plata with a surge height of more than 3 m, diminishing northward and southward. This area has one of the

largest ATs and the greatest average SS level (see **Fig. 3**), so MSL changes are insignificant in proportion to SS and tidal range.

Fig. 9 depicts the annual trends for the SS extremes (central panel), where only results over the 95% statistical significance level are shown. Seasonal behavior is also incorporated at certain representative points in the Figure. The results indicate that the zone with the greatest positive trend was that of Río de la Plata, with values of up to 5 mm/year between 1948 and 2008. This was also the area with the

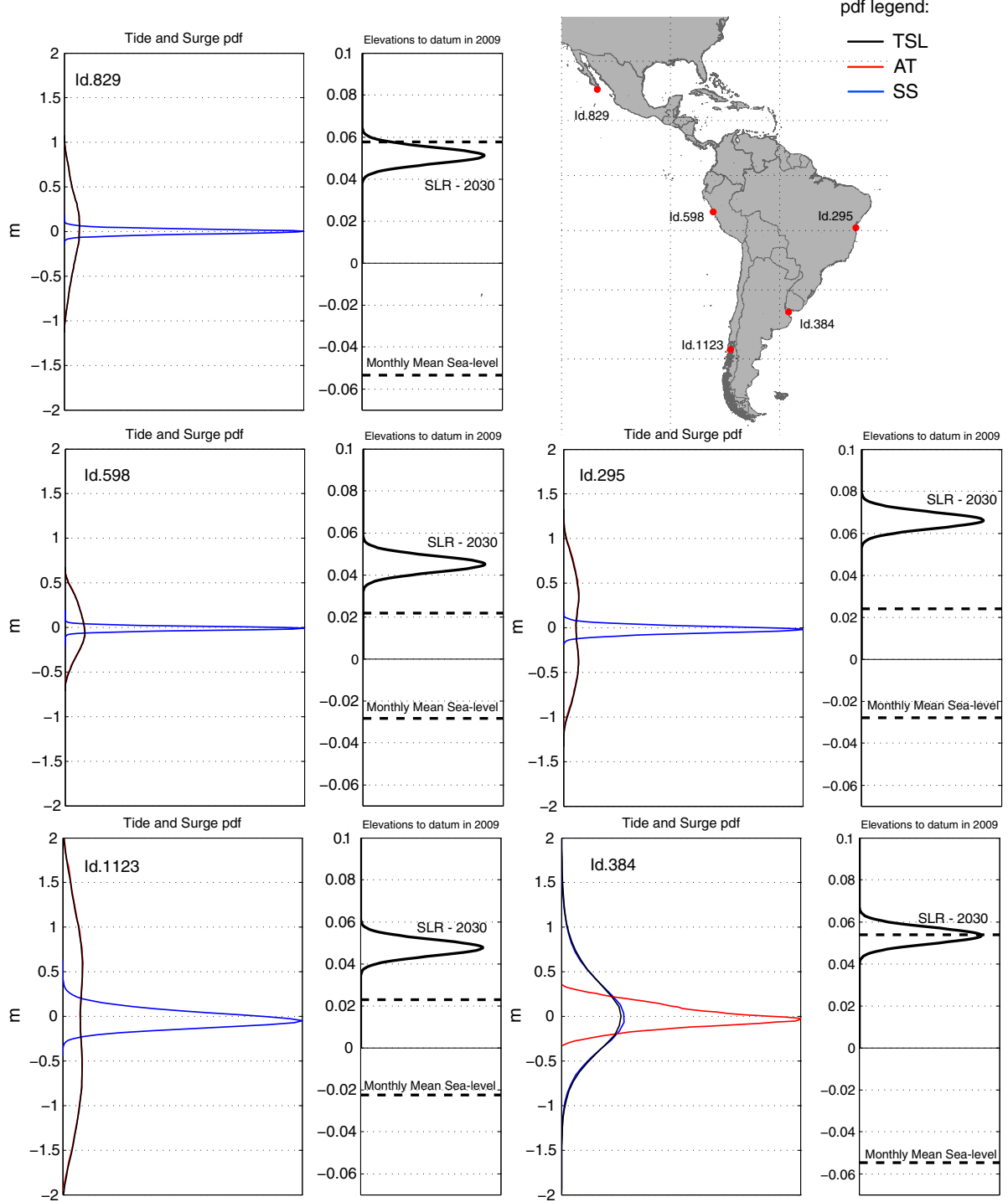


Fig. 10. Panels illustrating the relative weight of each sea-level component at various representative points. Panels on the left: probability density functions (pdf) of the Astronomical Tide (red), the Storm Surge (blue) and Total Sea-Level (black). Right panels: Mean Sea-Level seasonality range (broken black line) and probability density function of mean sea-level in 2030 from extrapolation of trends (solid black line). Note that when the red line (AT) is not seen, it is obscured by the black line (total sea level). TSL: Total Sea-Level; AT: Astronomical Tide; SS: Storm Surge; SLR: Sea-Level Rise.

greatest surge extremes, throughout all seasons. Trends decrease to 2 mm/year immediately southwards from the river inlet and reaching the southern Brazilian coast northwards. These results are in accordance with those in Fiore et al. (2009) which found seasonal increases in frequency of SS events and long-term trends of 2 mm/year from the Mar de Plata tidal gauge. A remarkable negative trend was found in the Gulf of California where the rate is approximately -3 mm/year, with a marked seasonality, dropping particularly during the Northern Hemisphere winters (DJF). A moderate (1.5 mm/year) increase in surge extremes was noted on the southern Brazilian coast along with a similar reduction in the northern coast. Seasonality was also marked in this zone. On the other coasts in the study area, trends were less than 1 mm/year, either increasing or decreasing, although always significant. No significant differences in extreme values were detected in the area affected by hurricanes and tropical storms,

although this result cannot be viewed as conclusive because the magnitude of the hurricane peaks is not well-represented in our analysis.

4.3. Relative influence of sea-level components

By aggregating the sea-level components, Fig. 10 shows the relative importance of each TSL contributor at various points. The panels on the left show the probability density functions (pdf) of AT, SS and TSL, while those on the right show the mean MSL seasonal range and the pdf of the MSL value for the year 2030 by extrapolating the calculated trends. These were designed to identify the proportion of the long-term change with respect to the seasonality, assuming that the acceleration observed up till now remains constant. The average regression estimator in the target year (2030) was obtained, to extrapolate the SLR value.

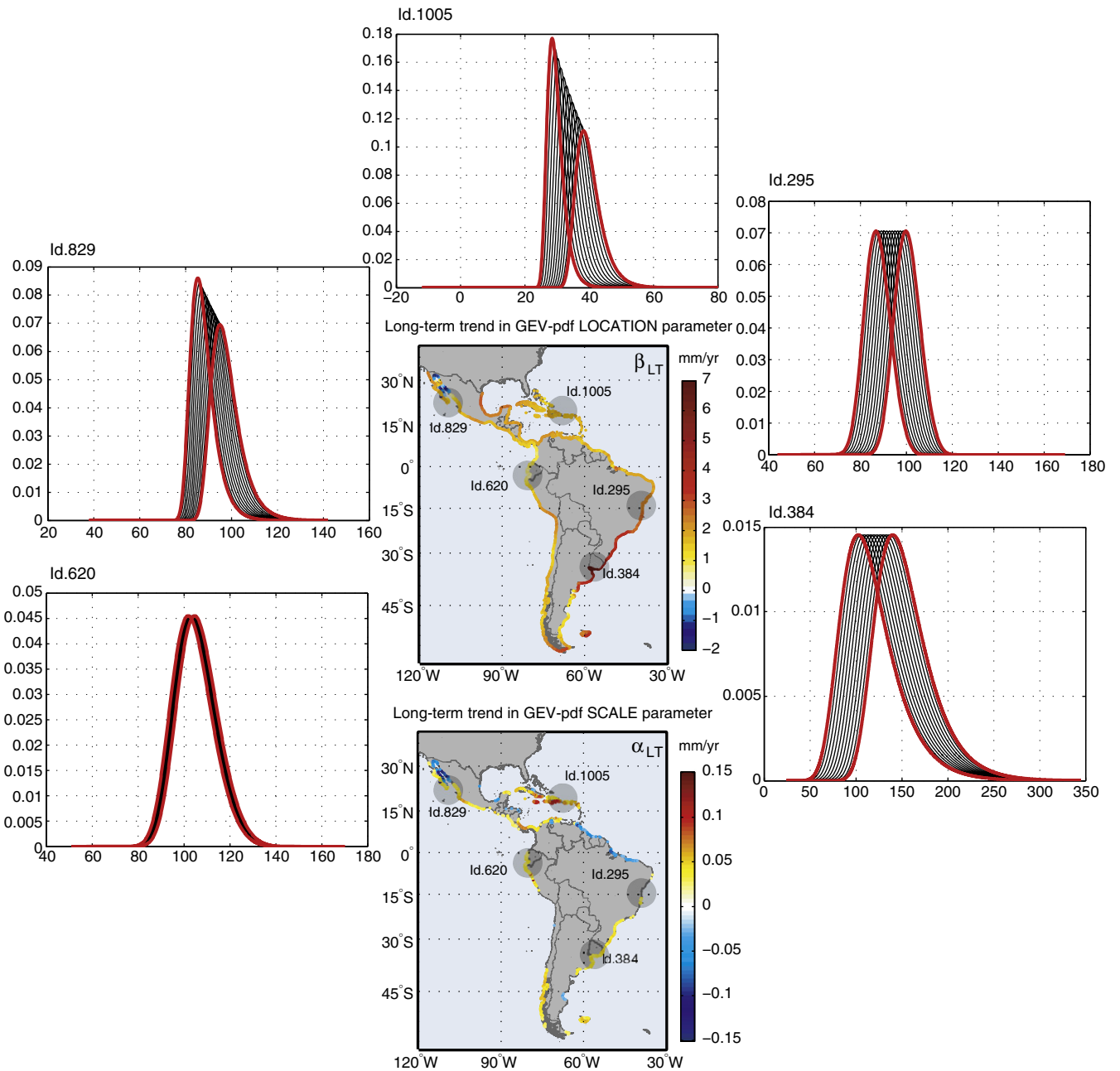


Fig. 11. Long-term trend coefficients of the location (upper panel) and scale (lower panel) parameters of the GEV probability density function of extreme levels of the Total Mean Sea-Level and temporal evolution of several probability density functions at certain points of study. Probability density functions are represented at 5 years intervals, the red lines corresponding to the initial (1950) and end (2008) years.

As shown in this figure, the AT generally dominates the TSL pdf except when the SS variation range is such that it surmounts astronomical influences, which only occurs in the Río de la Plata (point 384 in the figure). At the remaining locations, the SS variation range is below that of the AT, irrespective of tidal range (Fig. 10).

MSL seasonality also shifts spatially (between 4 cm and 12 cm on average), in proportion to the long-term trends. In areas where this seasonality is small (the tropical Atlantic coast and the south Pacific) SLR takes on greater importance. However, in macrotidal regions, because of the wide AT variation, the proportion of change due to SLR is marginal, i.e.: around 2.5% of change in the TSL range at point 1123 in southern Chile.

4.4. Changes in extreme total mean sea-levels

The stationary assumption is no longer valid (Milly et al., 2008), in a clear context of rising sea levels, and non-stationary extreme value approaches, which allows for the introduction of seasonal and long term variations, should be used to define the changes in extreme sea levels within decades. Results reveal that the coefficients of the location and scale parameters accounting for a long-term variation are significant for most of the points under study (maps in Fig. 11). The variation of the location parameter implies a shift in the average of the TSL pdf while the scale parameter change is related to a modification of its variance. The subsequent effect of the TSL pdfs varying in time (from 1950 to 2008) can be clearly detected in Fig. 11. Spatially, the pattern of trends reveals a large variability.

In general, trends in sea-level extremes (Fig. 11) rise by up to 7 mm/yr in the Río de la Plata area, in line with previously estimated MSL trends and SS extremes. Elsewhere in the region, trends ease to 2 mm/yr, with the MSL contributing predominantly over higher SSSs.

A slight reduction is noted in the Gulf of California, induced by negative trends in SS extremes.

Fig. 11 shows pdf variations in 5 year periods from 1950 at various representative locations. At sites with a long-term trend in the parameter of scale (e.g. point 1005) the pdf widens, making extreme values the most likely. At other points, particularly on the Atlantic coast, the trend in the parameter of scale was negligible (see the upper panels in Fig. 12), so that the pdf shift is driven solely by the trend in the shape parameter. Extreme values were also more frequent in these cases.

There were, nevertheless, points where no significant trends were found, neither in the scale nor in the location parameters, such as for example on the coast of Ecuador (i.e. Id. 620, Fig. 12). To provide further insight into this anomaly, Fig. 12 shows the temporal series of monthly maxima and the results of the adjusted parameters for two example points. In some cases (the top panels in Fig. 12) no significant long-term trends in extreme pdf parameters were found. Yet at other points (lower panels in the figure) this trend was significant for one or several parameters.

Long-term shifts in extreme pdfs suggest that extreme values have become more frequent in recent decades. However, it is now difficult to interpret the concept of return period because the average number of years between exceedances of TSL is continuously changing. For this reason, we calculate "equivalent stationary return period quantiles" for different years (Frías et al., 2012) during the two different decades associated with the initial and final time estimation period, i.e. 1950–1960 and 1998–2008, and then we average those return periods for each decade. The difference is shown in Fig. 13 and it is revealing. Comparisons between results allow us to easily understand the effect of sea level rise on return period estimation over all the estimation time frame.

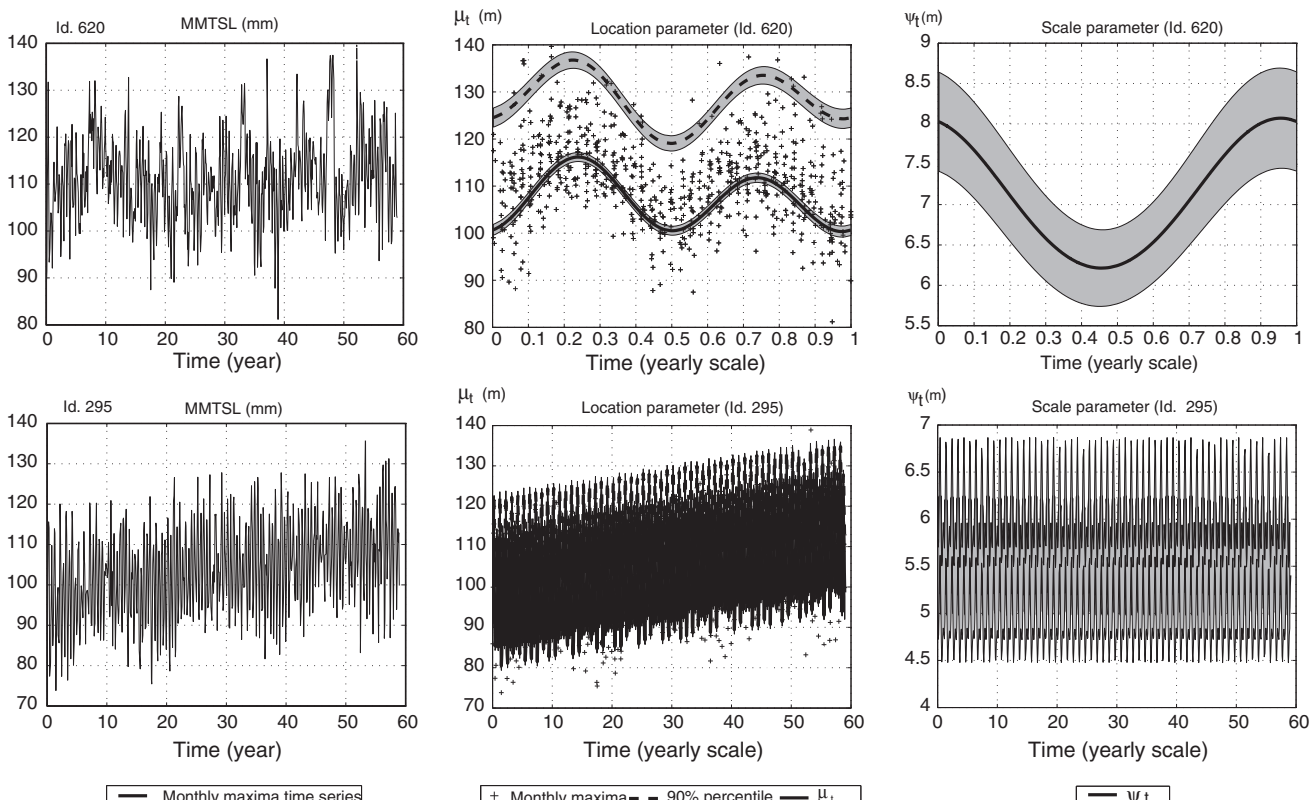


Fig. 12. Series of Monthly Maxima of Total Sea-Level (MMTSL; lines in left panels), location (central panels) and scale parameters (right panels) determined for two domain points: 620 (top panels) and 295 (bottom panels). The x-axis represents a temporal scale of years (years from 1950 to 2008 ranging from 1 to 59) when corresponding to time series in the left panels, and an annual scale (representing the months ranging from 0 to 1 year) when the trends were not significant (Id. 620). For the cases of the location and scale parameters (central and right panels), the crosses represent the monthly maxima data, the dashed line the 90th percentile, the continuous lines the fitted model and the shaded areas the 95% confidence intervals.

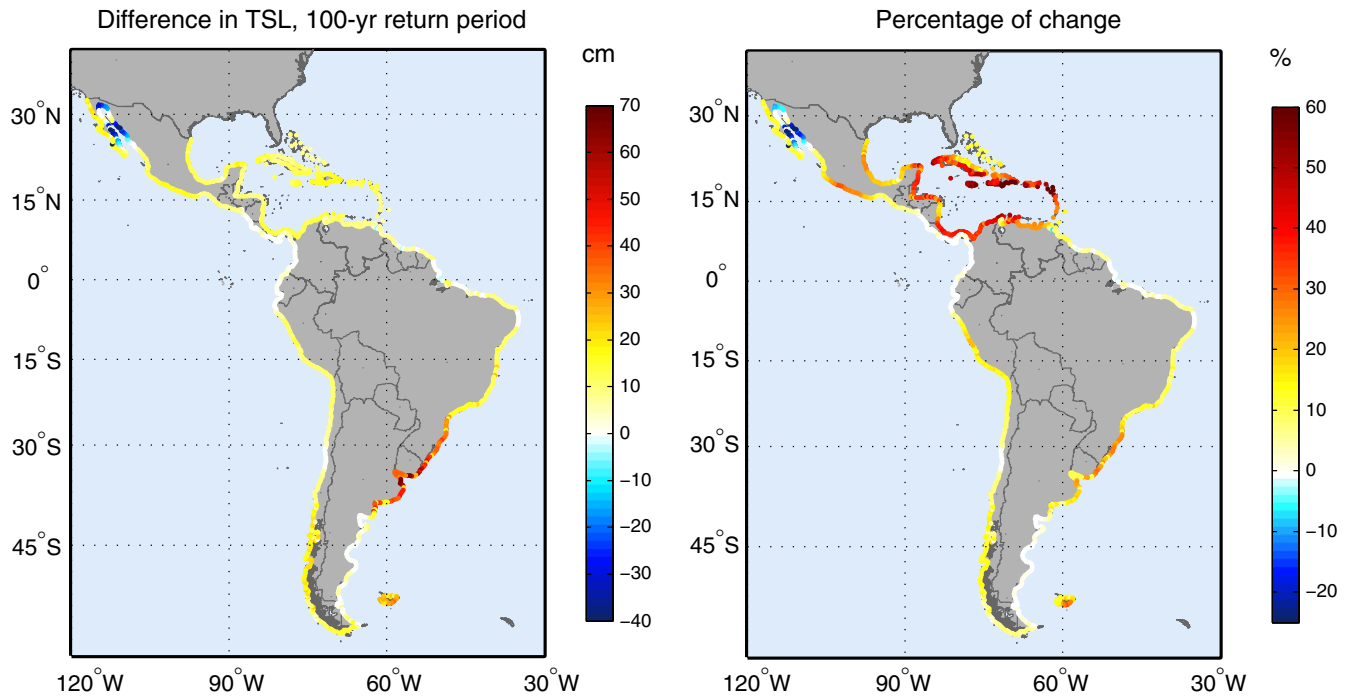


Fig. 13. Differences between 100-year return period sea-level values during the first (1950–60) and last decade (1998–2008) of available data (left panel). Percentage of change of such difference relative to the value associated with the 100-year return period obtained in the first decade of data (right panel).

The panel on the left shows the increase associated with the 100-year return period level, at its greatest in northern Argentina, Uruguay and southern Brazil, where the trend is dominated by SS extremes. At the remaining points, the MSL trend predominates and the change is not so obvious. However, if these differences are expressed in proportion to the value for the average return period between 1950 and 1960, the Caribbean islands saw this extreme value increase by more than 60% during that decade, compared with the 1998–2008 decade (with the aforementioned caution that hurricanes are not properly modeled in the peak magnitude of SS events).

These results imply that coastal flooding risk in low-lying areas may be increasing due to a combination of rising MSL and variations in SS extreme events. By itself, rising MSL may not cause flooding, but rising water levels have caused a decrease in the return periods of the extreme total water levels during the last five decades (Fig. 13). The proportion of these changes with respect to current dynamics (Fig. 10) will play an important role in impact evaluation and adaptation strategies.

5. Discussion of climate variability influence

As already seen in the MSL series, interannual variability arising from the ENSO phenomenon is, in some cases, clearly marked. Indeed, the ENSO phenomenon is known to have an effect on sea-levels in the Pacific Ocean (e.g., Liu et al., 2010; Walsh et al., 2012). Should changes in this climatic pattern occur (Collins et al., 2010) they will in turn influence sea-levels (Church et al., 2006; Lowe et al., 2010).

To analyze the influence of various climate patterns in sea-level components in the region of study, a number of climatic indices were considered: the Arctic oscillation (AO), the Southern Annular oscillation (SAM), the ENSO measured through the Niño3 index and the Southern Oscillation Index (SOI), the Pacific North American Index pattern (PNA), the Western Pacific Index (WP), the Eastern Pacific Oscillation (EP/NP), the Caribbean Sea Surface Temperature Index (CAR), Northeast Brazil rainfall (NBR), the North Tropical Atlantic Surface Temperature Index (NTA), the Tropical North Atlantic Index (TNA), and the Tropical Southern Atlantic Index (TSA). A comprehensive list

with definitions, descriptions and references can be found at <http://www.esrl.noaa.gov/psd/data/climateindices/list/>. The standardized series of the different climatic indices was correlated with the MSL and the 95th percentile of SS. Fig. 14 shows the Pearson correlation coefficients (varying between -1 and $+1$) at the points where correlation was significant, at least at the 95% confidence level. A cross correlation analysis was also performed (not shown) to identify patterns whose influence may be deferred in time because of the value of the climatic index and the maximum effect on sea-level on the coasts in the region of study.

Fig. 14 shows the correlation coefficient of the Niño3 climatic index with the normalized variables: MSL and the 95th percentile of SS. Niño3 showed the greatest correlation on sea-level components, as can be seen in the temporal series in Fig. 7, with a virtually simultaneous correlation (with no time lag). However, the correlation is also high for months with some time lag because the processes are of a large time scale (e.g., Smith, 1978; Meyers et al., 1998). The Niño3 index has a high correlation (correlation > 0.5), with standardized anomalies of MSL on the Pacific coast, between 15°S and 30°S on the Atlantic, and on the Caribbean islands. On the rest of region, the correlation was still positive but with lower values. Thus, Niño3 led to a generalized rise of sea-level throughout the study area, particularly on the continent's Pacific coast. Other indices such as TNA, CAR and AMO (not shown) also influenced sea-level anomalies significantly, although their correlations were lower.

Storm surge showed a correlation with Niño3 of 0.2, statistically significant for the entire Pacific coast. Positive values of this index are found to be related to a general rise in SS along the continent's Pacific façade, including the Caribbean islands and reaching the Gulf of Mexico where the correlation turns negative. On the Pacific coast, positive correlations are found west of the California peninsula and southwards, while the correlation becomes negative in the Gulf of California. Slightly negative values appear on parts of the tropical Atlantic coasts and Argentina. Concerning other indices (not shown), the influence of the NTA index is found to be positive on the Caribbean islands, and TSA is associated with negative rises between 15°N and 15°S on the Atlantic coast and in the Gulf of California.

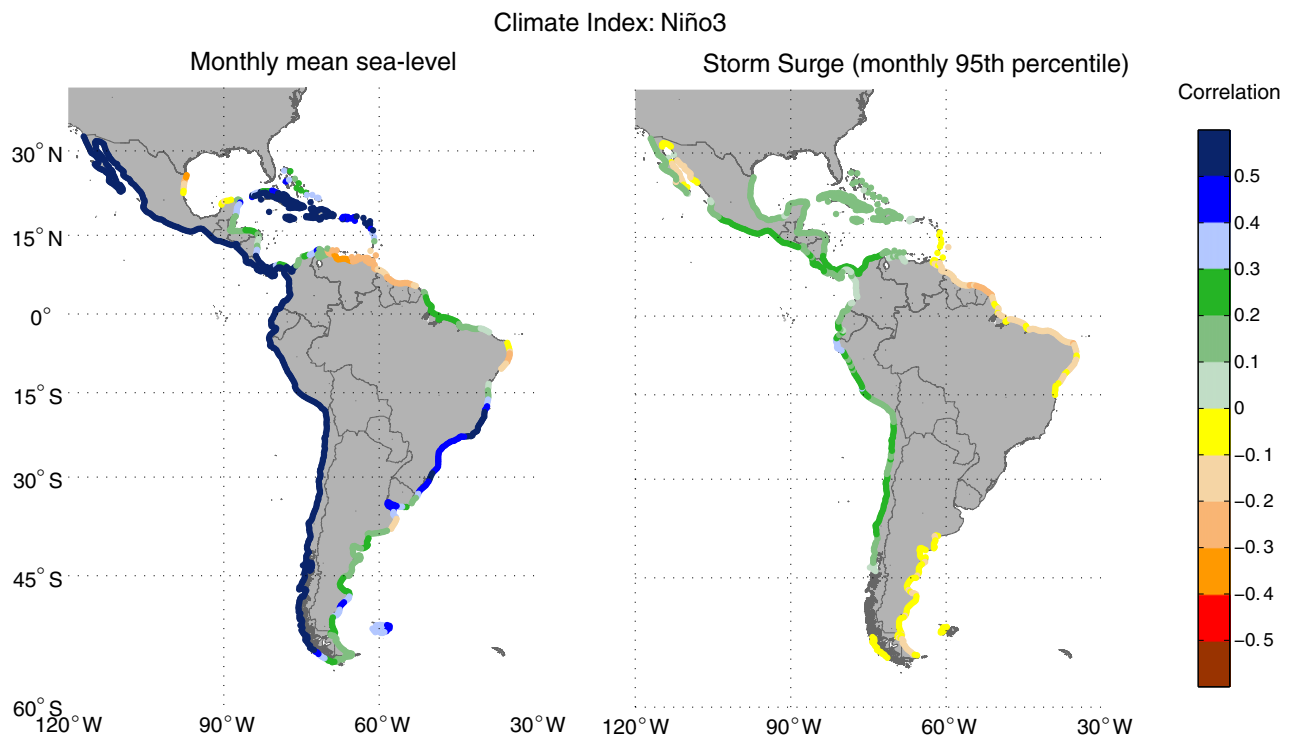


Fig. 14. Influence of Niño3 index in the Mean monthly Sea-Level (left panel) and the 95th percentile of Storm Surge (right panel) in terms of the Pearson's correlation coefficient. Only statistically significant results (based on a *t*-test) are shown.

In view of the correlation pattern, a study of the relationship between the Niño3 and the MSL was carried out. To determine the contribution of the Niño3 climate index to MSL, a simple regression model was built for the various points analyzed in the region. The results (shown in Fig. 15 for a representative point on the Peruvian coast) show a clear relationship (panel b in the figure), with the mean estimate of: $MSL (\text{mm}) = 30.47 \times \text{Niño3}^*$, where Niño3* represents the standardized climate index time series on a monthly scale. This simple model explains over 65% of the variance in MSL data (panel a). The predicted response confidence intervals represented for the regression (panel b) means that any new value of the Niño3 index would imply a MSL change within the represented bounds at a 95% confidence level. On average, the mean estimate corresponds to over 30 mm per unit of standardized index in a great part of the region (panel c), from 15°S to 15°N. The effect of Niño3 on the rest of the region is residual which may be indicating that a combination of climate patterns is occurring there.

6. Conclusions

This work provides a description of the various components of sea-level by constructing and analyzing time series of Astronomical Tide, Storm Surges and Mean Sea-Levels using different databases (both instrumental and numerical), for the region of Latin America and the Caribbean (LAC). In particular the Storm Surge reanalysis performed at a 0.25° spatial resolution in the study area must be highlighted. However, it must be noted that this contribution does not include an adequate description of hurricane events in the Caribbean, due to insufficient resolution in the forcing fields (taken from NCEP/NCAR reanalysis). With this in mind, during the period from 1950 to 2008 Storm Surge heights were largest in the area of Rio de la Plata, while the greatest Astronomical Tides occur in southern latitudes of the continent and in the Gulf of California.

The results obtained here are believed to provide useful insights in the determination of the probability of flooding in the coastal areas of

Latin America and the Caribbean, and they may also constitute an adequate approach for other areas of the world. As seen in this work, the variables contributing to total sea-level vary in importance at different coastal locations. Pinpointing the dominant variables, their changes, and their aggregated effect on coastal flooding, is thus crucial for coastal flood prevention and management.

With respect to the relative weight of each component on sea-level, certain features need to be highlighted. Past changes in sea-level present a higher weight in the Caribbean Islands in relation to the low range of tidal variability. This occurs together with a tail of distribution dominated by extreme events and associated with tropical storms and hurricanes. Despite the low rates of change detected and considering that conclusions from modeling must be taken with caution, extremes seems to have increased considerably in intensity during the last 5 decades, indicating a particular sensitivity in this area to smaller rises in water levels. This, together with the particular social, environmental and economic characteristics of the coastal zones in the islands should be a matter of concern and requires further research. The trends in water levels found in this region are negligible in comparison with the tidal ranges and the storm surge heights registered at extra-tropical areas. In these areas, flooding may be induced by changes in the storm surge regime, as a result of variations in the storm activity in the southern hemisphere, and coinciding with high tides. A remarkable exception is the Río de la Plata area where storm surge surpasses the tidal range, and so future changes in this component may be a major hazard for coastal zones in the area.

Owing to inter-annual changes in the region, like the ENSO phenomenon, which significantly affects certain areas of the LAC coasts, long-term trends in Mean Sea-Level data were computed using two different techniques: local regression and the Trend-EOF technique. Results were similar for most of the study area and in accordance with previous works at a global scale. However, the Trend-EOF approach provides a more uniform estimate for the whole region while revealing a lower trend in the tropical Pacific coast, consistent with trends calculated using local regression.

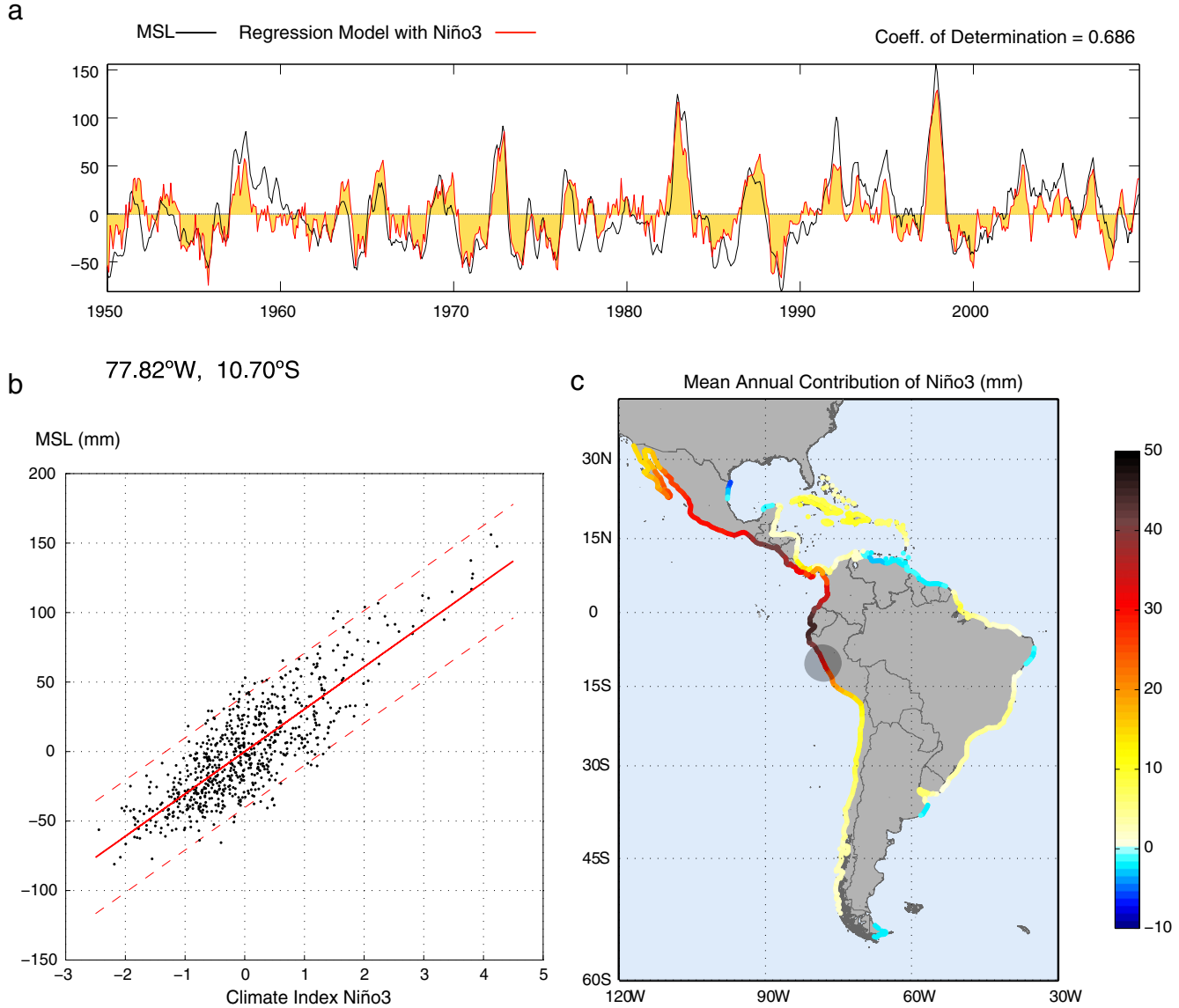


Fig. 15. (a) Sea-level time series at a point on the Pacific coast (77.82°W , 10.70°S) (black line), and time series reconstructed using the linear regression model with the Niño3 index (red line); (b) dispersion graph and regression line between the Niño3 index and Mean Sea-Level (mm), predicted response 95% confidence intervals are represented by dashed red lines; (c) average annual contribution to Mean Sea-Level (mm) per unit of Niño3 index (standardized index).

Storm surge monthly maxima were analyzed with a non-stationary extreme value model based on a GEV distribution accounting for long-term trends in location and scale parameters. An increasing SS trend of around 5 mm/year was found at the Rio de la Plata margin, precisely where Storm Surge events are of greatest concern. This is likely related to reported changes in the storm activity in the Southern Hemisphere (e.g., Fyfe, 2003). However, this analysis does not permit us to state if there is a linkage to climate variability indices since these were not included in the extremes model.

Building hourly time series of Total Sea-Level for the period 1950 to 2008 by aggregating the three components, the resulting data were analyzed with the non-stationary extreme analysis approach to identify long-term trends, which varied on average from 2 mm/year to 7 mm/year. The quantile associated with a 50-year return period was then computed and showed that it has been changing during the last decades due to modifications in probability density functions, which were spatially variable. Larger relative changes may be occurring in the southern Caribbean, notwithstanding the fact that the

hurricane tail of the distribution is not properly modeled in this analysis and that the largest changes in magnitude are found in the Rio de la Plata area. Indeed, up to 7 mm/yr were detected in storm surge past events in Rio de la Plata because of a clear translation in the mean value of the extreme probability density function. Meanwhile, in the Caribbean the probability density function of extremes of total sea-level are widening and translating, leading to higher probability for extremes.

El-Niño events are widely known to influence sea-levels in the Pacific Ocean. The highest historical event (1998) was in the same order of magnitude as the long-term change in Mean Sea-Level detected over the last 6 decades in the study region. This sets off the effects that variations in the ENSO phenomenon could entail as suggested by recent studies. In fact, a clear correspondence was found through a simple regression model between Mean Sea-Level and the Niño3 climate index, which in turn explained more than 65% of the variance in the signal and seemed to have an effect of over 30 mm per unit of standardized index in the tropical Pacific coast of LAC. The high tail of the Storm Surge distribution seems also to be related

to this and other climatic patterns but its assessment falls out of the scope of this work and was hence not evaluated.

Acknowledgements

The authors wish to acknowledge the NOAA — National Weather Service and the British Antarctic Survey for providing data on climate indices. The altimeter data were produced and distributed by AVISO (<http://www.aviso.oceanobs.com/>). B.G. Reguero is indebted to the University of Cantabria for funding. This work was partly funded by projects 'GRACCIE' (CSD2007-00067, Programa Consolider-Ingenio 2010) and 'IMAR21' (CTM201015009) from the Spanish Ministries of Economy and Agriculture, Food and Environment.

This work was part of the "Regional study on the effects of Climate Change in the coast of Latin America and the Caribbean" supported by the Economical Commission for Latin America and the Caribbean (ECLAC) from the United Nations (UN) and the Spanish Agency on Climate Change (OECC).

References

- Ardalan, A.A., Hashemi-Farahani, H., 2007. A harmonic approach to global ocean tide analysis based on TOPEX/POSEIDON satellite. *Marine Geophysical Research* 28, 235–255.
- Barbosa, S.M., 2008. Quantile trends in Baltic sea level. *Geophysical Research Letters* 35, L22704. <http://dx.doi.org/10.1029/2008GL035182>.
- Barbosa, S.M., Andersen, O.B., 2009. Trend patterns in global sea surface temperature. *International Journal of Climatology*. <http://dx.doi.org/10.1002/joc.1855>.
- Becker, M., Meyssignac, B., Letetrel, C., Llovel, W., Cazenave, A., Delcroix, T., 2012. Sea level variations at tropical Pacific islands since 1950. *Global and Planetary Change* 80–81, 85–98. <http://dx.doi.org/10.1016/j.gloplacha.2011.09.004>.
- Cazenave, A., Remy, F., 2011. Sea-level and climate: measurements and causes of changes. *WIREs Climate Change* 2, 647–662. <http://dx.doi.org/10.1002/wcc.139>.
- Cazenave, A., Lombard, A., Llovel, W., 2008. Present-day sea-level rise: A synthesis. *Oceanography Comptes Rendus Geoscience* 340, 761–770. <http://dx.doi.org/10.1016/j.crte.2008.07.008>.
- Chatterjee, S., Hadi, A.S., Price, B., 1990. *Regression Analysis by Example*. John Wiley & Sons, New York.
- Church, J., White, N., 2011. Sea-level rise from the late 19th to the early 21st century. *Surveys in Geophysics* 32 (4–5), 585–602. <http://dx.doi.org/10.1007/s10712-011-9119-1>.
- Church, J.A., White, N.J., Coleman, R., Lambeck, K., Mitrovica, J.X., 2004. Estimates of the regional distribution of sea-level rise over the 1950 to 2000 period. *Journal of Climate* 17, 2609–2625.
- Church, J.A., White, N.J., Hunter, J.R., 2006. Sea-level rise at tropical Pacific and Indian Ocean islands. *Global and Planetary Change* 53, 155–168. <http://dx.doi.org/10.1016/j.gloplacha.2006.04.001>.
- Clarke, Allan J., Van Gorder, Stephen, 1994. On ENSO coastal currents and sea levels. *Journal of Physical Oceanography* 24, 661–680. [http://dx.doi.org/10.1175/1520-0485\(1994\)024<0661:OECCAS>2.0.CO;2](http://dx.doi.org/10.1175/1520-0485(1994)024<0661:OECCAS>2.0.CO;2).
- Coles, S., 2001. An introduction to statistical modeling of extreme values. Springer Series in Statistics.
- Collins, M., An, S.I., Cai, W., Ganachaud, A., Guilyardi, E., Jin, F.-F., Jochum, M., Lengaigne, M., Power, S., Timmermann, A., Vecchi, G., Wittenberg, A., 2010. The impact of global warming on the tropical Pacific Ocean and El Niño. *Nature Geoscience* 3, 391–397. <http://dx.doi.org/10.1038/ngeo868>.
- Dasgupta, S., Laplante, B., Murray, S., Wheeler, D., 2009. Sea-level rise and storm surges: a comparative analysis of impacts in developing countries. Policy Research working paper n° 4901. The World Bank, Development Research Group - Environment and Energy Team.
- De Santis, A., Qamili, E., Spada, G., Gasperini, P., 2012. Geomagnetic South Atlantic anomaly and global sea-level rise: a direct connection? *Journal of Atmospheric and Solar-Terrestrial Physics* 74, 129–135. <http://dx.doi.org/10.1016/j.jastp.2011.10.015>.
- Egbert, G.D., Erofeeva, S.Y., 2002. Efficient inverse modeling of barotropic ocean tides. *Journal of Atmospheric and Oceanic Technology* 19, 183–204.
- Egbert, G.D., Bennett, A.F., Foreman, M.G.G., 1994. TOPEX/POSEIDON tides estimated using a global inverse model. *Journal of Geophysical Research* 99 (C12), 24821–24852.
- Ericson, J.P., Vorosmarty, C., Dingman, S., Ward, L., Meybeck, M., 2006. Effective sea-level rise and deltas: causes of change and human dimension implications. *Global and Planetary Change* 50, 63–82.
- Fiore, M.M.E., D'Onofrio, E.E., Pousa, J.L., Schnack, E.J., Bértola, G.R., 2009. Storm surges and coastal impacts at Mar del Plata, Argentina. *Continental Shelf Research* 29 (14), 1643–1649.
- Friás, M.D., Minguez, R., Gutiérrez, J.M., Méndez, F.J., 2012. Future regional projections of extreme temperatures in Europe: a nonstationary seasonal approach. *Climatic Change* 1–22. <http://dx.doi.org/10.1007/s10584-011-0351-y>.
- Fyfe, J.C., 2003. Extratropical Southern Hemisphere cyclones: harbingers of climate change. *Journal of Climate* 16, 2802–2805.
- Gazeaux, J., Flaounas, E., Naveau, P., Hannart, A., 2011. Inferring change points and nonlinear trends in multivariate time series: application to West African monsoon onset timings estimation. *Journal of Geophysical Research* 116, D05101. <http://dx.doi.org/10.1029/2010JD014723>.
- Hannachi, A., 2007. Pattern hunting in climate: a new method for finding trends in gridded climate data. *International Journal of Climatology* 27, 1–15. <http://dx.doi.org/10.1002/joc.1375>.
- Hong, B.G., Sturges, W., Clarke, A.J., 1999. Sea level on the U.S. East Coast: decadal variability caused by open ocean wind-curl forcing. *Journal of Physical Oceanography* 30, 2088–2098.
- IPCC (Intergovernmental Panel on Climate Change)Bindoff, N.L., Willebrand, J., Artale, V., Cazenave, A., Gregory, J., Gulev, S., Hanawa, K., Le Quéré, C., Levitus, S., Nojiri, Y., Shum, C.K., Talley, L.D., Unnikrishnan, A., 2007. Observations: oceanic climate change and sea level. In: Solomon, S., Qin, D., Manning, M., Chen, Z., Marquis, M., Averyt, K.B., Tignor, M., Miller, H.L. (Eds.), *Climate Change 2007: The Physical Science Basis. Contribution of Working Group I to the Fourth Assessment Report of the Intergovernmental Panel on Climate Change*. Cambridge University Press, Cambridge, United Kingdom and New York, NY, USA.
- Izaguirre, C., Méndez, F.J., Menéndez, M., Losada, I.J., 2011. Global extreme wave height variability based on satellite data. *Geophysical Research Letters* 38 (L10607).
- Jevrejeva, S., Grinsted, A., Moore, J.C., Holgate, S., 2006. Nonlinear trends and multiyear cycles in sea-level records. *Journal of Geophysical Research* 111, C09012. <http://dx.doi.org/10.1029/2005JC003229>.
- Kalnay, E., Kanamitsu, M., Cifster, R., Collins, W., Deaven, D., Gandin, L., Iredell, M., Saha, S., White, G., Woolen, J., Zhu, Y., Chelliah, M., Ebisuzaki, W., Higgins, W., Janowiak, J., Mo, K., Ropelewski, C., Wang, J., Leetmaa, A., Reynolds, R., Jenne, R., Joseph, D., 1996. The NCEP/NCAR reanalysis project. *Bulletin of the American Meteorology Society* 77, 437–471.
- Katz, R.W., Parlange, M.B., Naveau, P., 2002. Statistics of extremes in hydrology. *Advances in Water Resources* 25, 1287–1304.
- Lawrence, S.P., Llewellyn-Jones, D.T., Smith, S.J., 2004. The measurement of climate change using data from the advanced very high resolution and along track scanning radiometers. *Journal of Geophysical Research* 109, C08017.
- Li, Jianke, Clarke, Allan J., 2007. Interannual Sea Level variations in the south pacific from 5° to 28°S. *Journal of Physical Oceanography* 37 (12), 2882–2894. <http://dx.doi.org/10.1175/2007JPO3656.1>.
- Liu, X., Liu, Y., Guo, L., Rong, Z., Gu, Y., Liu, Y., 2010. Interannual changes of sea-level in the two regions of East China Sea and different responses to ENSO. *Global and Planetary Change* 72 (3), 215–226. <http://dx.doi.org/10.1016/j.gloplacha.2010.04.009>.
- Lowe, J.A., Gregory, J.M., 2005. The effects of climate change on storm surges around the United Kingdom. *Philosophical Transactions of the Royal Society A: Mathematical, Physical and Engineering Sciences* 363 (1831), 1313–1328. <http://dx.doi.org/10.1088/rsta.2005.1570>.
- Lowe, J.A., Woodworth, P.L., Knutson, T., McDonald, R.E., McInnes, K.L., Wothon, K., von Storch, H., Wolf, J., Swail, V., Bernier, N.B., Gulev, S., Horsburgh, K.J., Unnikrishnan, A.S., Hunter, J.R., Weisse, R., 2010. Past and Future Changes in Extreme Sea Levels and Waves. In: Church, J.A., Woodworth, P.L., Aarup, T., Wilson, W.S. (Eds.), *Understanding Sea-Level Rise and Variability*. Wiley-Blackwell, Oxford, UK. <http://dx.doi.org/10.1002/9781444323276.ch11>.
- McInnes, K.L., O'Grady, J.G., Hubbard, G.D., 2009. Modeling sea level extremes from storm surges and wave setup for climate change assessments in southeastern Australia. *Journal of Coastal Research* SI56, 1005–1009.
- Menéndez, M., Woodworth, P.L., 2010. Changes in extreme high water levels based on a quasiglobal tide-gauge data set. *Journal of Geophysical Research* 115, C10011. <http://dx.doi.org/10.1029/2009JC005997>.
- Menéndez, M., Méndez, F.J., Izaguirre, C., Luceño, A., Losada, I.J., 2009. The influence of seasonality on estimating return values of significant wave height. *Coastal Engineering* 56 (3), 211–219.
- Meyers, S.D., Melsom, A., Mitchum, G.T., O'Brien, J.J., 1998. Detection of the Fast Kelvin Wave Teleconnection due to El Niño southern oscillation. *Journal of Geophysical Research – Oceans* 103 (C12), 27655–27663.
- Meyssignac, B., Cazenave, A., 2012. Sea level: a review of present-day and recent-past changes and variability. *Journal of Geodynamics* 58, 96–109. <http://dx.doi.org/10.1016/j.jog.2012.03.005>.
- Milly, P.C.D., Betancourt, J., Falkenmark, M., Hirsch, R.M., Kundzewicz, Z.W., Lettenmaier, D.P., Stouffer, R.J., 2008. Stationarity is dead: whither water management? *Science* 319, 573–574.
- Minguez, R., Méndez, F.J., Izaguirre, C., Menéndez, M., Losada, I.J., 2010. Pseudo-optimal parameter selection of non-stationary generalized extreme value models for environmental variables. *Environmental Modelling & Software* 25, 1592–1607.
- Nerem, R.S., Chambers, D.P., Leuliette, E.W., Mitchum, G.T., Giese, B.S., 1999. Variations in global mean sea level associated with the 1997–1998 ENSO event: Implications for measuring long term sea level change. *Geophysical Research Letters* 26 (19), 3005–3008. <http://dx.doi.org/10.1029/1999GL002311>.
- Nicholls, R.J., 2011. Planning for the impacts of sea-level rise. *Oceanography* 24 (2), 144–157. <http://dx.doi.org/10.5670/oceanog.2011.34>.
- Nicholls, R.J., Cazenave, A., 2010. Sea-level rise and its impact on coastal zones. *Science* 328, 1517–1520. <http://dx.doi.org/10.1126/science.1185782>.
- Reguero, B.G., Menéndez, M., Méndez, F.J., Minguez, R., Losada, I.J., 2012. A global Ocean Wave (GOW) calibrated reanalysis from 1948 onwards. *Coastal Engineering* 65, 38–55. <http://dx.doi.org/10.1016/j.coastaleng.2012.03.003>.
- Reguero, B.G., Méndez, F.J., Losada, I.J., 2013. Variability of multivariate wave climate in Latin America and the Caribbean. *Global and Planetary Change* 100, 70–84. <http://dx.doi.org/10.1016/j.gloplacha.2012.09.005>.
- Rice, J., 1994. *Mathematical Statistics and Data Analysis*. Duxbury Press, Boston.

- Rignott, E., Velicogna, I., van den Broeke, M.R., Monaghan, A., Lenaerts, J.T.M., 2011. Acceleration of the contribution of the Greenland and Antarctic ice sheets to sea-levelrise. *Geophysical Research Letters* 38, L05503. <http://dx.doi.org/10.1029/2011GL046583>.
- Rust, H.W., Maraun, D., Osborn, T.J., 2009. Modeling seasonality in extreme precipitation. A UK case study. *European Physics Journal, Special Topics* 174, 99–111.
- Schepetkin, A.F., MacWilliams, J.C., 2003. A method for computing horizontal pressure-gradient force in an oceanic model with a nonaligned vertical coordinate. *Journal of Geophysical Research* 108 (C3), 3090. <http://dx.doi.org/10.1029/2001JC001047>.
- Smith, R.L., 1978. Poleward Propagating Perturbations in Currents and Sea Levels Along the Peru Coast. *Journal of Geophysical Research* 83 (C12), 8C0836.
- Sturges, W., Hong, B.G., 1995. Wind forcing of the Atlantic Thermocline along 32°N at low frequencies. *Journal of Physical Oceanography* 25, 1706–1715. [http://dx.doi.org/10.1175/1520-0485\(1995\)025<1706:WFOTAT>2.0.CO;2](http://dx.doi.org/10.1175/1520-0485(1995)025<1706:WFOTAT>2.0.CO;2).
- Sturges, W., Hong, B.G., Clarke, Allan J., 1998. Decadal wind forcing of the North Atlantic subtropical gyre. *Journal of Physical Oceanography* 28, 659–668. [http://dx.doi.org/10.1175/1520-0485\(1998\)028<0659:DWFOTN>2.0.CO;2](http://dx.doi.org/10.1175/1520-0485(1998)028<0659:DWFOTN>2.0.CO;2).
- Syvitski, J.P.M., Kettner, A.J., Overeem, I., Hutton, E.W.H., Hannon, M.T., Brakenridge, G.R., Day, J., Vörösmarty, C., Saito, Y., Giosan, L., Nicholls, R.J., 2009. Sinking deltas due to human activities. *Nature Geoscience* 2, 681–686.
- Tsimplis, M.N., Woodworth, P.L., 1994. The global distribution of the seasonal sea-level cycle calculated from coastal tide gauge data. *Journal of Geophysical Research* 99, 16,031–16,039.
- Walsh, K.J.E., McInnes, K.L., McBride, J.L., 2012. Climate change impacts on tropical cyclones and extreme sea levels in the South Pacific area – a regional assessment. *Global and Planetary Change* 80–81, 149–164. <http://dx.doi.org/10.1016/j.gloplacha.2011.10.006>.
- Weatherhead, E.C., Reinsel, C., Tiao, G.C., Meng, X., Choi, D., Cheang, W., Keller, T., DeLisi, J., Wuebbles, D.J., Kerr, J.B., Miller, A.J., Oltmans, S.J., Frederick, J.E., 1998. Factors affecting the detection of trends: statistical considerations and applications to environmental data. *Journal of Geophysical Research* 103 (D14), 17149–17161.
- Weatherhead, E.C., Stevermer, A.J., Schwartz, B.E., 2002. Detecting environmental changes and trends. *Physics and Chemistry of the Earth, Parts A/B/C* 27 (6–8), 399–403.
- Whiteman, D.N., Vermeesch, K.C., Oman, L.D., Weatherhead, E.C., 2011. The relative importance of random error and observation frequency in detecting trends in upper tropospheric water vapor. *Journal of Geophysical Research D: Atmospheres* 116 (21), D21118. <http://dx.doi.org/10.1029/2011JD016610>.